

Energy Dependence of Profile Functions in $p\bar{p}$ and pp Scattering

A. K. Kohara, E. Ferreira, and T. Kodama

Instituto de Física, Universidade Federal do Rio de Janeiro

C.P. 68528, Rio de Janeiro 21945-970, RJ, Brazil

(Dated: April 1, 2024)

We construct analytical forms in the impact parameter b -space for the real and imaginary amplitudes describing elastic pp and $p\bar{p}$ scattering. The amplitudes converted analytically to the momentum transfer t -space have magnitudes, slopes, curvatures, zeros, signs, obeying phenomenological and theoretical expectations, and describe with high precision all details of the data, in the full- t range, and for energies from 20 GeV to 7 TeV. The connection of forward with large- $|t|$ behavior allows precise determination of total cross-sections, slopes and other scattering parameters. We study the properties and the energy dependence of the b -space profile functions, observing that the real part has fundamental influence in the structure of $d\sigma/dt$ at intermediate and large $|t|$ values. We discuss the 540/546 GeV and 1.8/1.96 TeV data from CERN SPS and Fermilab TEVATRON and the 7 TeV results from TOTEM measurements at LHC, and investigate the extrapolation to 14 TeV and higher energies.

I. INTRODUCTION AND MOTIVATION

The differential cross sections of elastic pp and $p\bar{p}$ scattering are described by two amplitudes, $T_R(s, t)$ and $T_I(s, t)$, through

$$\frac{d\sigma}{dt} = (\hbar c)^2 |T_R(s, t) + iT_I(s, t)|^2. \quad (1)$$

Two amplitude functions contain basic information on the proton structure and are represented by two kinematical variables (s, t) only: this simplicity gives charm and importance of the elastic scattering process. In spite of the this simplicity, and of the 40 years of measurements and theories, the real and imaginary terms are not known well enough. Microscopic models have not been precise and clarifying enough for the separate identification of the two parts. In the present work, the data on pp and $p\bar{p}$ elastic scattering at high energies are described in terms of real and imaginary amplitudes with high accuracy in the whole t -range, within a formalism including the expectation of dispersion relation for amplitudes and for slopes. This treatment leads also to a determination of the total cross section and other forward scattering parameters, permitting to investigate the compatibility of data and estimates. The identification of real and imaginary parts leads to values for slopes B_R and B_I of the real and imaginary amplitudes, that are independent quantities, influence the amplitudes in the whole t -range and are important for the determination of the total cross section. The amplitudes are fully constructed analytically both in impact parameter and momentum transfer spaces, and investigation is made of their extension to very large $|t|$, to include the universal contribution of the perturbative process of three gluon exchange.

The analysis shows the importance of the real part that, although having small contribution to the integrated elastic cross section, is crucial in the description of the details of the data at intermediate and high $|t|$. Our description leads to a prediction for a marked dip in $d\sigma/dt$ of $p\bar{p}$ elastic scattering in the $|t|$ range 3 - 5 GeV²

at the energies 0.546 and 1.8 TeV due to the cancellation between the perturbative real term of negative sign and the real non-perturbative contribution of positive sign in this region.

Coulomb interference is treated properly, with the Coulomb phase derived taking into account the difference in slopes of the real and imaginary amplitudes. In the 541/546 GeV case, the data of event rate at very low $|t|$ are submitted to the Coulomb interference forms, and normalization connection with absolute differential cross section is obtained. The low $|t|$ data for $d\sigma/dt$ thus constructed is joined to the data of other measurements, and a continuous and consistent data-basis is obtained for analysis.

In the 1.8/1.96 TeV case, the forward scattering data of the E-710 and CDF experiments are joined to the recent D0 Collaboration points at large $|t|$, and attempts are made to find unified treatments of the experimental information.

II. ANALYTICAL FORM OF PROFILE FUNCTIONS

To establish a bridge connecting data to theory, the amplitudes T_R and T_I must be determined phenomenologically as functions of s and t . This is a disentanglement problem, which in principle has no completely model-independent solution. However, we believe that our efforts lead to, possibly realistic, representations for the amplitudes, as functions of $|t|$ in their full intervals, for each of the measured energies with minimal dependence on a specific model.

In practical terms, we need to propose analytical representations for imaginary and real parts, proving that they cover with accuracy all $|t|$ ranges present in the data. At a given energy, the determination of fundamental parameters such as total cross section, slopes, ρ ratio, depend on limits $|t| \rightarrow 0$ evaluated with specific functions $T_R(s, t)$ and $T_I(s, t)$. These forms must

have curvatures, zeros, magnitudes, signs, that build the whole observed $d\sigma/dt$ structure. It is fundamental that precise reproduction of the data be obtained, with regular evolution between neighbor experimental energies. Theoretical constructions should be checked against the imaginary and real terms, which must be considered as necessary and reliable bridge between data and models.

We propose [1] analytical forms in the impact parameter b -space

$$\tilde{T}_K(s, b) = \frac{\alpha_K}{2\beta_K} e^{-\frac{b^2}{4\beta_K}} + \lambda_K \tilde{\psi}_K(s, b), \quad (2)$$

where

$$\tilde{\psi}_K(s, b) = \frac{2e^{\gamma_K}}{a_0} \frac{e^{-\sqrt{\gamma_K^2 + \frac{b^2}{a_0}}}}{\sqrt{\gamma_K^2 + \frac{b^2}{a_0}}} \left[1 - e^{\gamma_K} e^{-\sqrt{\gamma_K^2 + \frac{b^2}{a_0}}} \right] \quad (3)$$

is a shape function. The indices $K = I$ and $K = R$ in $\tilde{T}_K(s, b)$ refer to the real and imaginary parts. The form introduced in Eq.(3) has origin in studies with the Stochastic Vacuum Model [2], and four energy-dependent parameters have been introduced for each amplitude.

We note that $\tilde{\psi}_K(s, b = 0) = 0$, so that $\tilde{T}_K(s, b = 0) = \alpha_K/2\beta_K$.

The amplitudes $T_R(s, t)$ and $T_I(s, t)$ given as functions of the momentum transfer $|t|$ are obtained through Fourier transforms

$$\tilde{T}_K(s, b) = \frac{1}{2\pi} \int d^2\vec{q} e^{-i\vec{q}\cdot\vec{b}} T_K^N(s, t = -q^2). \quad (4)$$

One of the advantages of this representation is that it permits analytic representation also in t space [1].

The connection with the quantities used in the description of forward scattering are

$$\sigma(s) = 4\sqrt{\pi}(\hbar c)^2 (\alpha_I(s) + \lambda_I(s)), \quad (5)$$

$$\rho(s) = \frac{T_R^N(s, t = 0)}{T_I^N(s, t = 0)} = \frac{\alpha_R(s) + \lambda_R(s)}{\alpha_I(s) + \lambda_I(s)}, \quad (6)$$

and

$$B_K(s) = \frac{1}{T_K^N(s, t)} \frac{dT_K^N(s, t)}{dt} \Big|_{t=0} = \frac{1}{\alpha_K(s) + \lambda_K(s)} \times \left[\alpha_K(s)\beta_K(s) + \frac{1}{8}\lambda_K(s)a_0(6\gamma_K(s) + 7) \right]. \quad (7)$$

We stress the importance of different values allowed for the imaginary and real parts of the complex amplitude, as required by dispersion relations [3].

In the numerical analysis of data we work directly with the amplitudes in t -space because they are more directly connected to the $d\sigma/dt$ measurements. Using as units milibarns for cross sections and GeV^2 for the momentum transfer squared t , we have $(\hbar c)^2 = 0.389 \text{ mb GeV}^2$.

These expressions represent the non-perturbative dynamics of scattering for all $|t|$. For very large $|t|$ there is also a contribution of a perturbative tail representing 3-gluon exchange, which is assumed to be universal, independent of the energy. It has been first observed [4] at 27.4 GeV, and gives a $|t|$ dependence of the form $1/|t|^8$ in $d\sigma/dt$ [5].

An important consequence of the precise description of $d\sigma/dt$ in terms of amplitudes valid for all $|t|$ is that we determine the total cross section and the slope parameters with precision based on the whole set of data points in t . In this way we can observe more clearly the origin of discrepancies in reported values of σ that occur, historically, at 541/546 GeV and at 1.8/1.96 TeV. This question is recalled in Fig 1, where parts of the plots in the Review of Particle Properties of the Particle Data Group [6] are reproduced. We stress that in most cases total cross sections are not determined by direct measurements, but extracted from the measured elastic scattering distributions by some extrapolation procedures or model dependent calculations. It must be remarked that the publications of the experimental groups have taken care to distinguish the experimental and calculated information in separate papers.

The variety of reported values of cross sections at 0.546

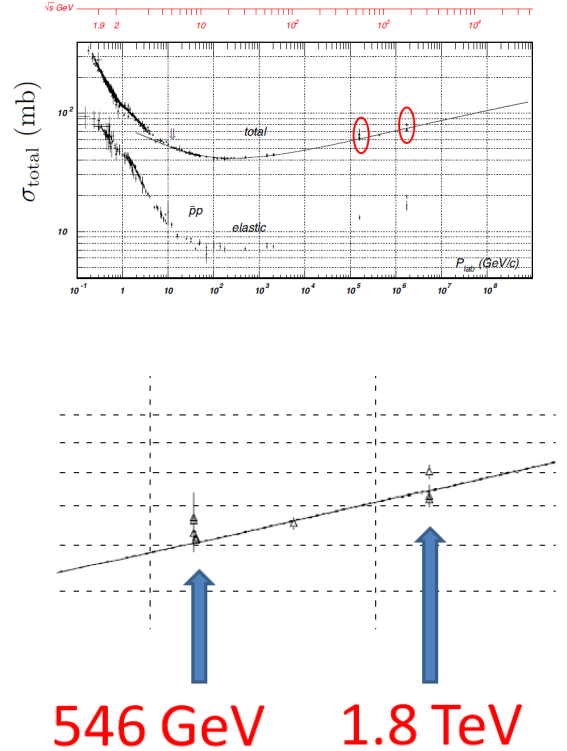


FIG. 1. Plots of total pp and $p\bar{p}$ cross sections in the Review of Particle Properties of the Particle Data Group.

and 1.8 TeV are shown in Fig. 2.

III. ANALYSIS OF DATA AT HIGH ENERGIES

A. $\sqrt{s} = 7$ TeV

The fitting [7] of the 165 points of the TOTEM measurements at 7 TeV [8] is shown in Fig. 3. To show the regularity of the method, we plot together the results for 52.8 GeV. Parameters are given in the tables.

The presence of a perturbative tail for very large $|t|$ beyond 5 GeV² [4] is observed a 52.8 GeV and predicted for 7 TeV, as shown in the second part of the same figure.

B. $\sqrt{s} = 1.8/1.96$ TeV

The $d\sigma/dt$ data of the E-710 [9], CDF [10] and D0 [11] experiments are shown in Fig. 4. The line shown in the figure is a fitting of a basis of 52 points formed with the E-710 and D0 data. Numerical values of the parameters of this line are given in the tables.

A complete analysis of all data at 1.8 and 1.96 TeV [12] comparing results obtained with different sets of data, taken from E-710, CDF [10] and D0 experiments

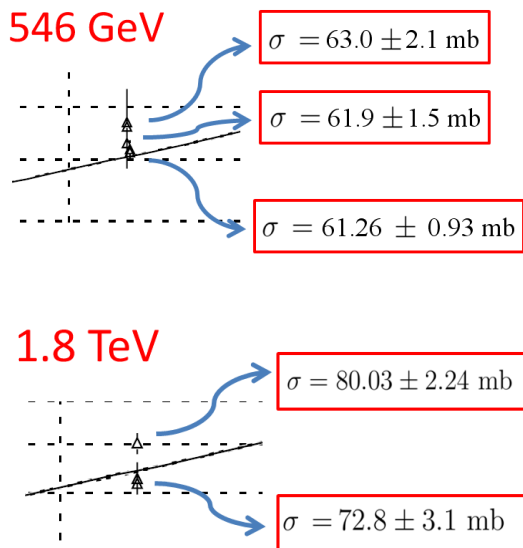


FIG. 2. Variety of values of total cross sections at 0.546 and 1.8 TeV reported in literature [6]. We believe that the large error bars result from methods concentrating on forward scattering points, ignoring independence of slopes of amplitudes and using a single exponential form for $d\sigma/dt$. We stress that in general, total cross sections are not direct measurements, but rather are calculated values based on elastic scattering data. We thus remark that a more complete treatment of all elastic scattering data is necessary, as done in our work.

at Fermilab suggests separate treatments in three different datasets, which reduces the discrepancies in values of the total cross section, but still points to the need of a judgment about the conditions of the two conflicting experiments made at Fermilab in the first years of the 1990 decade.

C. $\sqrt{s} = 0.546$ TeV

At 546 GeV the best quality data come from the UA4 experiment [13–15], with 121 points, which unfortunately do not reach the very low $|t|$ region. There are low $|t|$ data by Bernard et al. [16] and event rate points (not normalized) by Augier et al. [17]. We treat all these

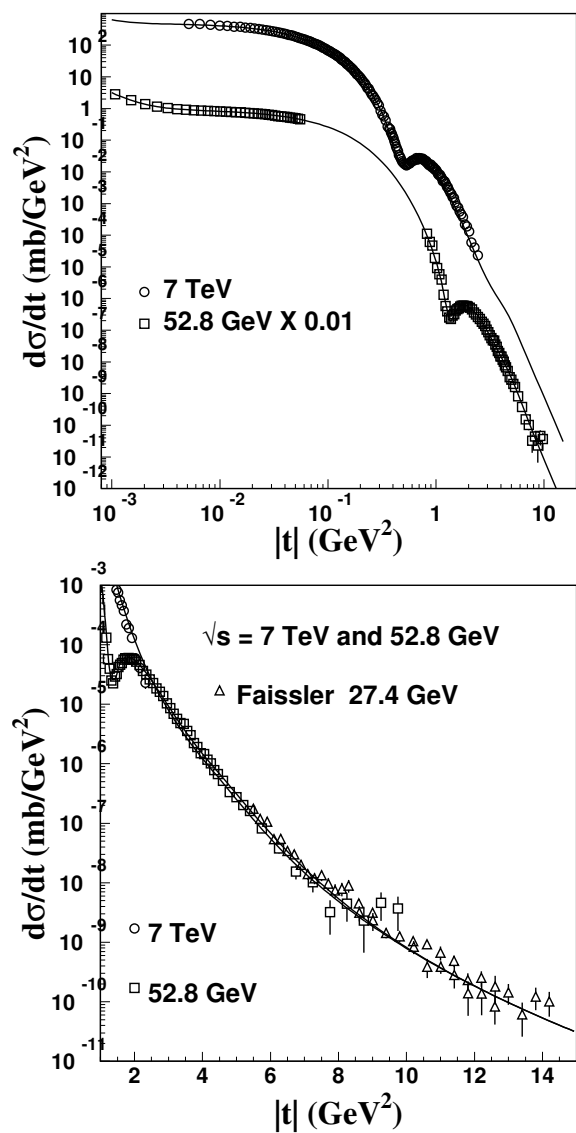


FIG. 3. Description of the data of $d\sigma/dt$ at 7 TeV and 52.8 GeV. The assumed connection with the universal tail at large $|t|$ is pointed out in the second plot, where it looks like natural.

measurements in a unified way, with a description of high precision, shown in Fig. 5, where the $\log(t)$ plots are used to enhance the forward region. The numerical values are given in the tables.

IV. AMPLITUDES AND PROFILE FUNCTIONS

The forms of the amplitudes are exemplified for the 7 TeV case [7] in Fig. 6.

We call attention for the important difference in slopes of T_I and T_R and to the features that are general in our solution for the disentanglement: one zero for the imaginary part, and two zeros for the real part in pp

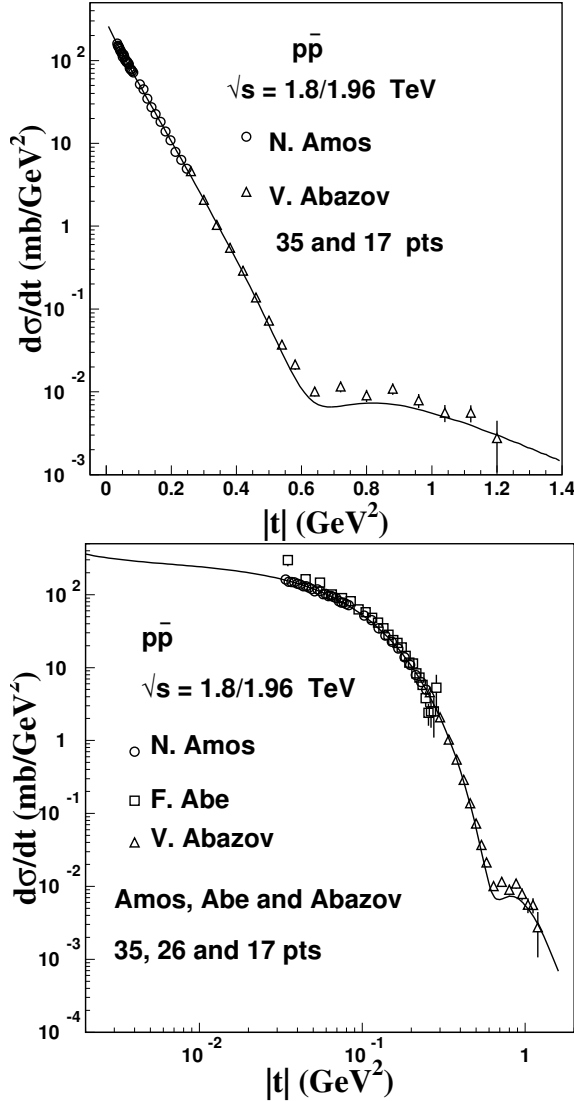


FIG. 4. Data of the E-710 [9], CDF [10] and D0 [11] experiments at 1.8/1.96 TeV. The line is a fit of a basis of 52 points formed with E-710 and D0 data [12]. The parameters are given in the tables, and the amplitudes in b -space are plotted in Fig. 8.

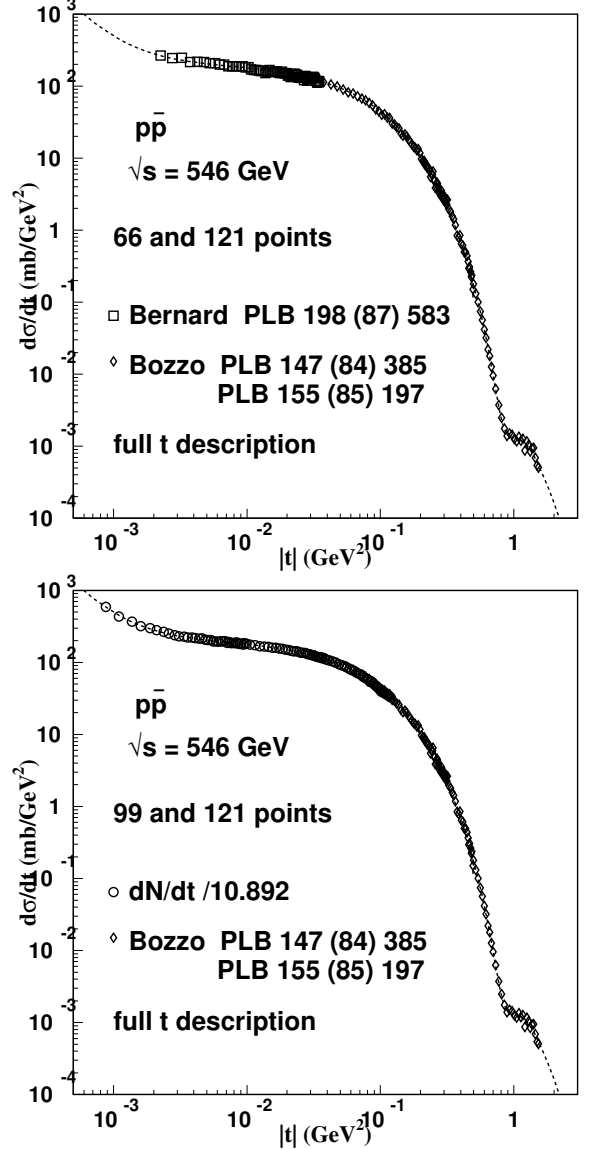


FIG. 5. The low $|t|$ points of the Bernard et al. [16] and event rate [17] measurements, put together with the points of Bozzo et al [13–15] enrich the description of the differential cross section at 546 GeV and allows a more precise determination of scattering parameters. The description of two different assemblages is consistent, with same parameter values, that are given in the tables. The amplitudes in b -space are plotted in Fig. 8.

scattering. In the $p\bar{p}$ case there may be a third real zero due to the negative contribution of the perturbative tail.

It is important to observe that for large $|t|$ the real and imaginary amplitudes (nuclear part) decrease, with positive and negative signs respectively.

See also Fig. 7

The amplitudes in b -space for several energies are shown in Fig. 8. Both $\tilde{T}_I(s, b)$ and $\tilde{T}_R(s, b)$ are always positive and fall to zero at large b more slowly than Gaussians. The magnitudes of \tilde{T}_R are always smaller than

TABLE I. Free Independent Parameters

\sqrt{s} TeV	N points	imaginary amplitude				real amplitude				$\langle\chi^2\rangle$
		σ mb	B_I GeV $^{-2}$	α_I GeV $^{-2}$	β_I GeV $^{-2}$	ρ	B_R GeV $^{-2}$	λ_R GeV $^{-2}$	β_R GeV $^{-2}$	
0.0307	201	40.38	12.47	6.0180	2.3437	0.036	25.0	0.5226	0.8	2.430
0.0446	230	41.84	13.10	6.0953	2.4321	0.0545	18.0	0.7823	0.96	1.940
0.0528	97	42.49	13.04	5.9561	2.3477	0.078	19.07	1.1307	1.1436	0.8328
0.0625	138	43.25	13.20	5.9202	2.3336	0.086	19.0	1.2480	1.3282	2.284
0.546	180	62.00	15.37	10.363	3.4336	0.1350	22.00	2.8849	1.00	1.0807
0.9		65.30	16.0	10.80	3.6	0.138	23.0	3.13	1.05	
1.8	52	72.76	16.76	11.62	3.7633	0.1415	24.00	3.5400	1.15	1.3412
7	165	98.65	19.77	13.730	4.0826	0.141	30.20	4.7525	1.4851	0.3105
14		108	21.0	14.4	4.3	0.141	32.0	5.17	1.50	
57		131	22.0	16.3	4.7	0.141	35.0	6.3	1.6	

TABLE II. Derived properties of amplitudes and cross sections

\sqrt{s} TeV	Z_I GeV 2	$Z_R(1)$ GeV 2	$Z_R(2)$ GeV 2	$ t _{\text{dip}}$ GeV 2	$ t _{\text{bump}}$ GeV 2	ratio	$T_I(b=0)$ GeV 2	$T_R(b=0)$ GeV 2	$\sigma(\text{el,Real})$ mb	$\sigma(\text{el})$ mb	$\sigma(\text{inel})$ mb	$\sigma(\text{el})/\sigma$
0.0307	1.4016	0.1828	1.6079	1.4039	1.8794	79.95	1.2839	0.0028	0.004	7.070	33.31	0.1751
0.0447	1.3364	0.2874	1.6607	1.3733	1.8107	3.710	1.2531	0.0232	0.014	7.183	34.66	0.1717
0.0528	1.3083	0.2710	1.6157	1.3560	1.7947	3.281	1.2685	0.0310	0.028	7.431	35.06	0.1749
0.0625	1.2794	0.2797	1.6201	1.3365	1.7562	2.606	1.2685	0.0380	0.036	7.593	35.66	0.1756
0.546	0.8282	0.2282	1.2551	1.0005	1.0005	1	1.5091	0.0750	0.156	13.402	48.60	0.2162
0.9	0.7425	0.2170	1.1970	0.8897	0.8897	1	1.5000	0.0768	0.175	14.210	51.09	0.2176
1.8	0.6336	0.2080	1.1337	0.6946	0.8133	1.079	1.5439	0.0840	0.216	16.694	56.07	0.2294
7	0.4671	0.1641	0.8235	0.4847	0.6488	1.838	1.6815	0.0980	0.311	25.542	35.06	0.2589
14	0.4251	0.1568	0.7097	0.4371	0.5999	2.395	1.7093	0.1172	0.350	28.70	79.30	0.2657
57	0.3285	0.1411	0.6608	0.3314	0.5019	6.172	1.7340	0.1242	0.470	39.53	91.47	0.3017

those of \tilde{T}_I , differently from what happens in t space, where there are zeros and variations in magnitudes.

The integrated elastic cross section from the real part is much smaller than the corresponding value for the imaginary part, but the its presence is crucial for the design of the $d\sigma/dt$ form at intermediate and large t values.

V. TABLES AND ENERGY DEPENDENCE

The very regular behavior observed in the plots of the amplitudes in Fig. 8 is seen also in their characteristic parameters. This is shown in Figs. 9 and 11.

The quantities characteristic of the forward range (total cross-section, ρ parameter and slopes) for the energies of the data, are shown in Fig. 11. The extrapolations to the very high energy of the Auger cosmic rays experiment are interesting, giving total cross section value compatible with the evaluation by the experimental group [20].

In our scheme, at all energies the imaginary part has only one zero. The second zero of the real amplitude has important role in the behavior of $d\sigma/dt$ at intermediate and large $|t|$ values.

VI. SUMMARY AND PERSPECTIVES

In this work we report results of detailed analyses of experimental data on pp and p \bar{p} elastic scattering cross section in terms of their amplitudes for the highest energies available. In spite of the simplicity of the form of the profile amplitudes, which originates on applications of the stochastic vacuum model, our analytic representation reproduces the experimental data with remarkable precision in the whole t domain, from the very forward scattering to the structure and position of dips and bumps, further still allowing extension to the tail domain where the perturbative three gluon exchange mechanism is expected to dominate.

It is found that the energy dependence of the fitted parameters is quite regular as function of $\ln s$, showing that they can carry important information on QCD dynamics and proton structure.

When compared to the description obtained for lower ISR energy data, we still observe smooth connection, although deflection in some interpolated lines may suggest possible additional changes in curvatures occurring in the energy range $100 \text{ GeV} \leq \sqrt{s} \leq 500 \text{ GeV}$. The occurrence of disturbed regularity may happen if some new channels in the final state of pp or p \bar{p} collisions start to open in this energy range (for example, emergence of deconfined quark-gluon droplets). This phenomenon would starts to

increase the inelastic and the total cross sections. Thus, through the optical theorem, elastic cross section would also be affected. Therefore, emergence of such a critical behavior should reflect in the change in curvature of parameters as function of energy. Unfortunately, there exist no data points for this energy domain. We expect that pp experimental data in the RHIC energies could have a decisive role for the understanding the QCD dynamics at the critical region.

The identification of the imaginary and real amplitudes

here presented may provide a framework for development and control of ingredients of microscopic theoretical models that study the underlying dynamics.

ACKNOWLEDGMENTS

The authors wish to thank CNPq, PRONEX and FAPERJ for financial support.

-
- [1] E. Ferreira and F. Pereira, *Phys. Rev. D* **59**, 014008 (1998) ; *Phys. Rev. D* **61**, 077507 (2000).
 - [2] H.G. Dosch, *Phys. Lett. B* **190**, 177 (1987) ; H.G. Dosch, E. Ferreira, A. Kramer *Phys. Rev. D* **50**, 1992 (1994).
 - [3] E. Ferreira, Int. Jour. Mod. Phys. E **16**, 2893 (2007).
 - [4] W. Faissler et al. *Phys. Rev. D* **23**, 33 (1981).
 - [5] A. Donnachie, P. Landshoff, *Zeit. Phys. C* **2**, 55 (1979); *Phys. Lett. B* **387**, 637 (1996).
 - [6] J. Beringer et al. (Particle Data Group), *Phys. Rev. D* **86**, 010001 (2012).
 - [7] A. Kendi Kohara, E. Ferreira and T. Kodama, *Eur. Phys. J. C* **73**, 2326 (2013).
 - [8] G. Antchev et al.(TOTEM Collaboration), *Europhys. Lett.* **95**, 41001 (2011); id *Europhys. Lett.* **96**, 21002 (2011); Rept no.CERN-PH-EP-2012-239 (data extraction is available in link <http://hepdata.cedar.ac.uk/view/red2659>, Durham Data Basis); M.G. Ryskin, A. D. Martin and V. A. Khoze, *Eur. Phys. J. C* **72**, 1937 (2012); I. M. Dremin and V. A. Nechitailo, *Phys. Rev. D* **85**, 074009 (2012).
 - [9] N. Amos et al, Fermilab E-710 Coll, *Phys. Lett. B* **262**, 127, (1990).
 - [10] F. Abe et al. , Fermilab CDF Coll., *Phys. Rev. D* **50**, 5518 (1994).
 - [11] V. M. Abazov et al, D0 Coll., *Phys. Rev. D* **86**, 012009 (2012).
 - [12] A. K. Kohara, E. Ferreira and T. Kodama, *Phys. Rev. D*, **87**, 054024 (2013).
 - [13] M. Bozzo et al.,UA4 Coll., *Phys. Lett.B* **147**, 385 (1984).
 - [14] M. Bozzo et al.,UA4 Coll.,*Phys. Lett.B* **155**, 197 (1985).
 - [15] M. Bozzo et al.,UA4 Coll.,*Phys. Lett.B* **147**, 392 (1985).
 - [16] D. Bernard et al.,UA4 Coll.,*Phys. Lett.B* **198**, 583 (1987).
 - [17] C. Augier et al, *Phys. Lett.B* **316**, 448 (1993).
 - [18] N. Amos et al. *Phys. Rev. Lett.* **68**, 2433 (1992); C. Avila et al., *Phys. Lett.B* **537**, 41 (2002) .
 - [19] F. Abe et al. *Phys. Rev. D* **50**, 5550 (1994).
 - [20] Auger Coll., *Phys. Rev. Lett.* **109**, 062002 (2012).
 - [21] C. Bourrely, J.Soffer and T.T. Wu, *Eur. Phys. J. C* **71**, 1601 (2011); C. Bourrely, J.M. Myers, J.Soffer and T.T. Wu, *Phys. Rev. D* **85**, 096009 (2012).

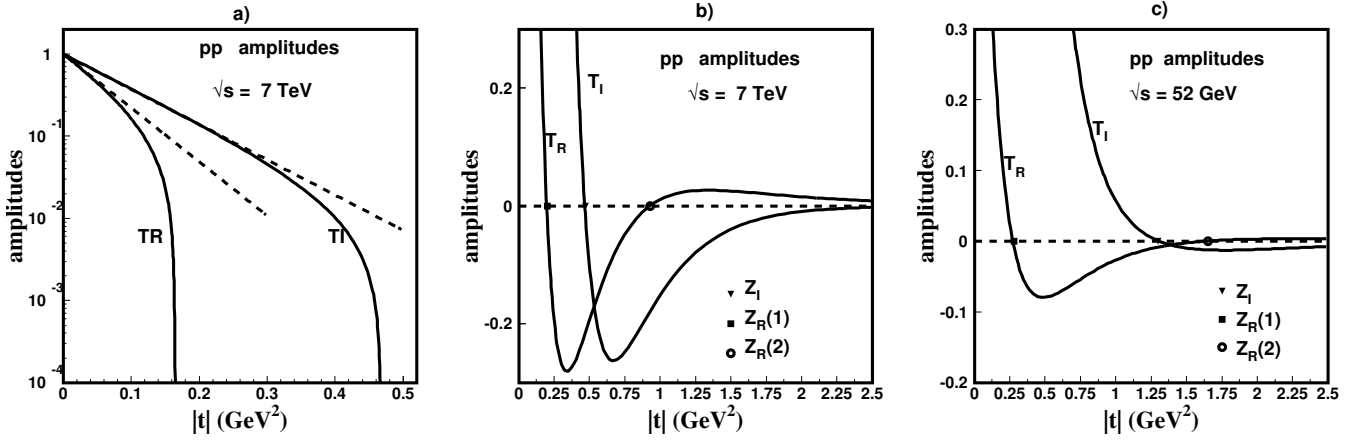


FIG. 6. (a) Forward scattering amplitudes T_R and T_I at $\sqrt{s} = 7$ TeV in log scale, normalized to one at $|t| = 0$, showing their slopes, $B_I = 19.77$ and $B_R = 30.2 \text{ GeV}^{-2}$, and their curvatures, and indicating positions of the first zeros $Z_R(1)$ and Z_I ; (b) Large- t dependence of the real and imaginary scattering amplitudes showing the complete set of zeros; (c) t dependence of the real and imaginary scattering amplitudes at $\sqrt{s} = 52.8$ GeV. Comparing with the figure for 7 TeV, we observe that all zeros move towards smaller $|t|$ values as the energy increases.

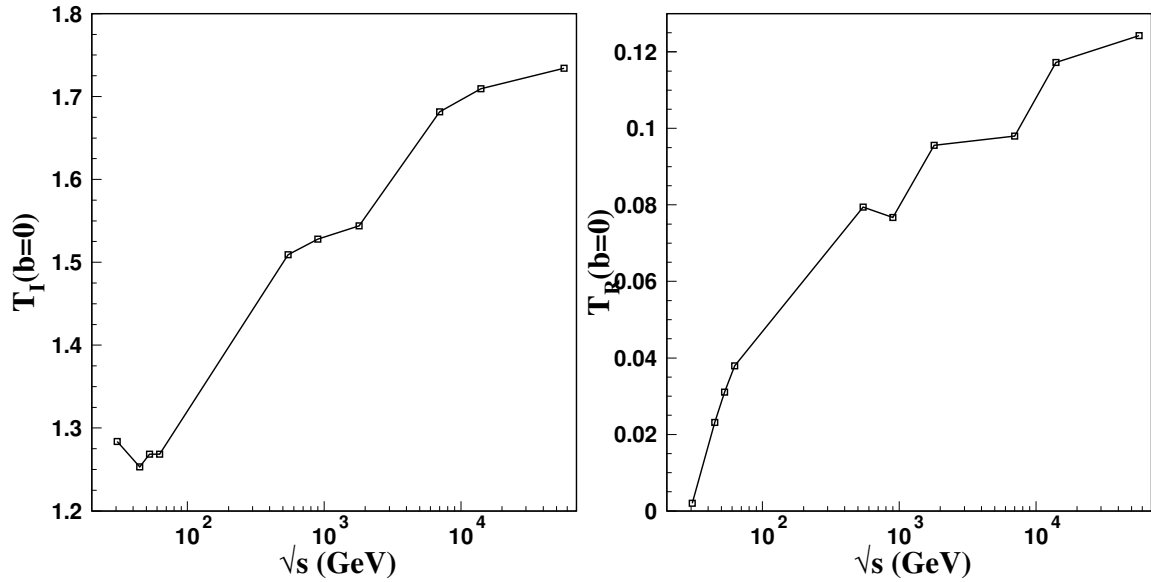


FIG. 7. Values of the imaginary and real profile functions at $b = 0$.

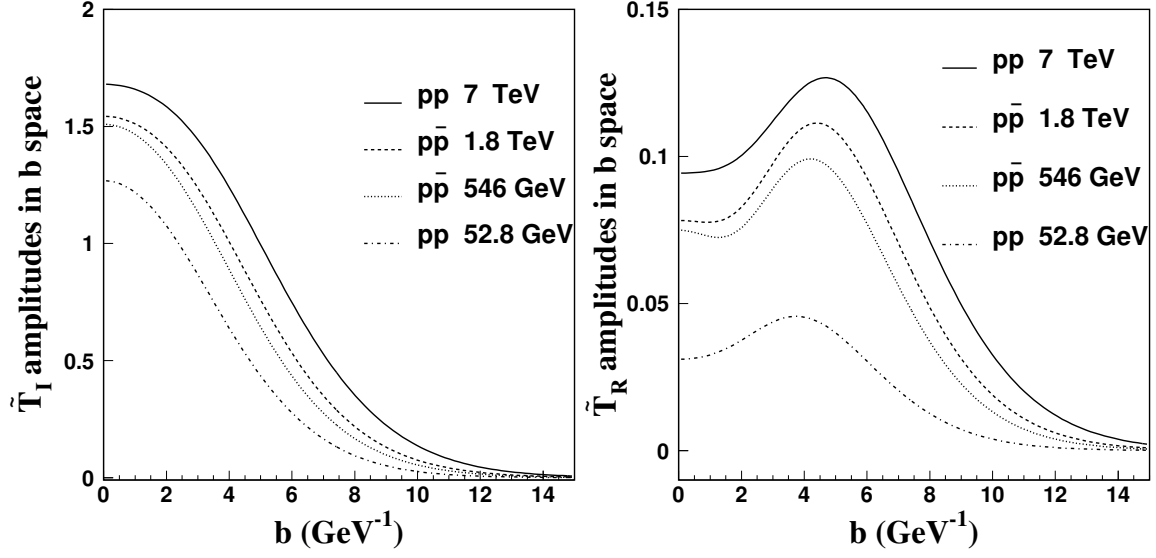


FIG. 8. Imaginary and real amplitudes in impact parameter space, for several energies. The regularity of the evolution of the functions as the energy varies is impressive.

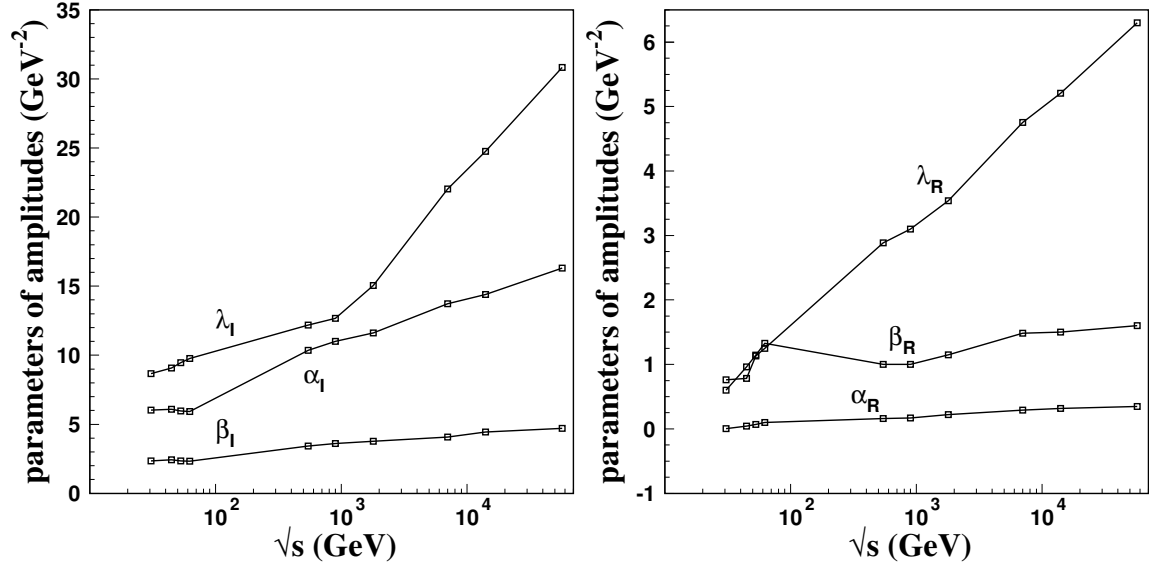


FIG. 9. Parameters of the amplitudes at the energies of the data. In each case, the fourth free parameter is the corresponding slope, B_I or B_R , shown in the next figure. The sum $\alpha_I + \lambda_I$ gives the total cross section in GeV^{-2} , and the sum $\alpha_R + \lambda_R$ gives the real amplitude at $|t| = 0$, equal to $\rho \times \sigma$.

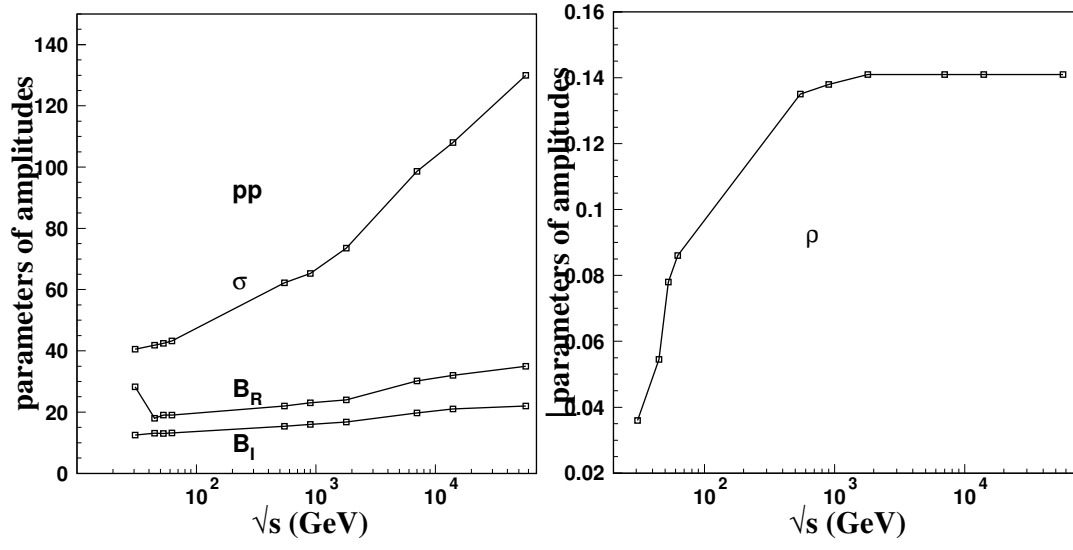


FIG. 10. Total cross-section and slopes characteristic of forward scattering; the ρ parameter.

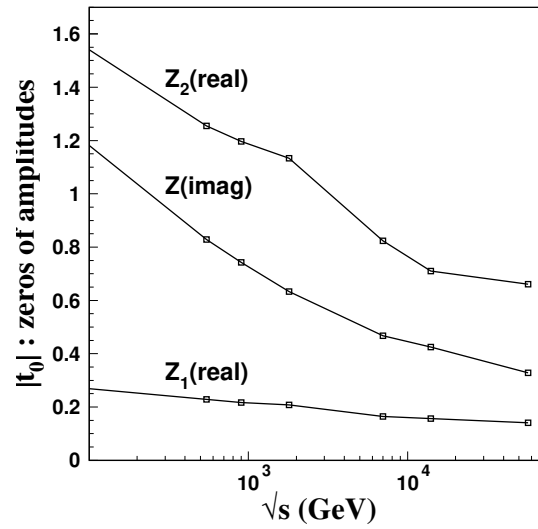


FIG. 11. Positions of zeros of the amplitudes.